



Citation for published version:

Morris, AM, Kocevski, DD, Trump, JR, Weiner, BJ, Hathi, NP, Barro, G, Dahlen, T, Faber, SM, Finkelstein, SL, Fontana, A, Ferguson, HC, Grogin, NA, Grützbauch, R, Guo, Y, Hsu, L-T, Koekemoer, AM, Koo, DC, Mobasher, B, Pforr, J, Salvato, M, Wiklind, T & Wuyts, S 2015, 'A WFC3 Grism Emission Line Redshift Catalog in the GOODS-South Field', *Astronomical Journal*, vol. 149, no. 6. <https://doi.org/10.1088/0004-6256/149/6/178>

DOI:

[10.1088/0004-6256/149/6/178](https://doi.org/10.1088/0004-6256/149/6/178)

Publication date:

2015

Document Version

Peer reviewed version

[Link to publication](#)

(C) 2015 American Astronomical Society. This is an Author's Accepted Manuscript of an article published in Morris, AM, Kocevski, DD, Trump, JR, Weiner, BJ, Hathi, NP, Barro, G, Dahlen, T, Faber, SM, Finkelstein, SL, Fontana, A, Ferguson, HC, Grogin, NA, Grützbauch, R, Guo, Y, Hsu, L-T, Koekemoer, AM, Koo, DC, Mobasher, B, Pforr, J, Salvato, M, Wiklind, T & Wuyts, S 2015, 'A WFC3 Grism Emission Line Redshift Catalog in the GOODS-South Field' *Astronomical Journal*, vol 149, no. 6., and available online via: <http://dx.doi.org/10.1088/0004-6256/149/6/178>

University of Bath

General rights

Copyright and moral rights for the publications made accessible in the public portal are retained by the authors and/or other copyright owners and it is a condition of accessing publications that users recognise and abide by the legal requirements associated with these rights.

Take down policy

If you believe that this document breaches copyright please contact us providing details, and we will remove access to the work immediately and investigate your claim.

A WFC3 GRISM EMISSION LINE REDSHIFT CATALOG IN THE GOODS-SOUTH FIELD

AARON M. MORRIS¹, DALE D. KOCEVSKI¹, JONATHAN R. TRUMP^{2,3}, BENJAMIN J. WEINER⁴, NIMISH P. HATHI⁵, GUILLERMO BARRO⁶, TOMAS DAHLEN⁷, SANDRA M. FABER⁶, STEVEN L. FINKELSTEIN⁸, ADRIANO FONTANA⁹, HENRY C. FERGUSON⁷, NORMAN A. GROGIN⁷, RUTH GRÜTZBAUCH^{10,11}, YICHENG GUO^{6,12}, LI-TING HSU¹³, ANTON M. KOEKEMOER⁷, DAVID C. KOO⁶, BAHRAM MOBASHER¹⁴, JANINE PFORR^{15,16}, MARA SALVATO¹³, TOMMY WIKLIND⁷, STIJN WUYTS¹³

Draft version February 11, 2015

ABSTRACT

We combine *HST*/WFC3 imaging and G141 grism observations from the CANDELS and 3D-HST surveys to produce a catalog of grism spectroscopic redshifts for galaxies in the CANDELS/GOODS-South field. The WFC3/G141 grism spectra cover a wavelength range of $1.1 \leq \lambda \leq 1.7 \mu\text{m}$ with a resolving power of $R \sim 130$ for point sources, thus providing rest-frame optical spectra for galaxies out to $z \sim 3.5$. The catalog is selected in the *H*-band (F160W) and includes both galaxies with and without previously published spectroscopic redshifts. Grism spectra are extracted for all *H*-band detected galaxies with $H \leq 24$ and a CANDELS photometric redshift $z_{\text{phot}} \geq 0.6$. The resulting spectra are visually inspected to identify emission lines and redshifts are determined using cross-correlation with empirical spectral templates. To establish the accuracy of our redshifts, we compare our results against high-quality spectroscopic redshifts from the literature. Using a sample of 411 control galaxies, this analysis yields a precision of $\sigma_{NMAD} = 0.0028$ for the grism-derived redshifts, which is consistent with the accuracy reported by the 3D-HST team. Our final catalog covers an area of 153 arcmin² and contains 1019 redshifts for galaxies in GOODS-S. Roughly 60% (608/1019) of these redshifts are for galaxies with no previously published spectroscopic redshift. These new redshifts span a range of $0.677 \leq z \leq 3.456$ and have a median redshift of $z = 1.282$. The catalog contains a total of 234 new redshifts for galaxies at $z > 1.5$. In addition, we present 20 galaxy pair candidates identified for the first time using the grism redshifts in our catalog, including four new galaxy pairs at $z \sim 2$, nearly doubling the number of such pairs previously identified.

Subject headings: catalogs, galaxies: high-redshift, techniques:spectroscopic

1. INTRODUCTION

aaron.morris2@uky.edu

¹Department of Physics and Astronomy, University of Kentucky, Lexington, KY 40506

²Department of Astronomy and Astrophysics, Pennsylvania State University, University Park, PA 16802

³Hubble Fellow

⁴Steward Observatory, 933 N. Cherry Street, University of Arizona, Tucson, AZ 85721, USA

⁵Aix Marseille Université, CNRS, LAM (Laboratoire d'Astrophysique de Marseille) UMR 7326, 13388, Marseille, France

⁶UCO/Lick Observatory and Department of Astronomy and Astrophysics, University of California, Santa Cruz, CA 95064 USA

⁷Space Telescope Science Institute, Baltimore, MD 21218, USA

⁸The University of Texas at Austin, 2515 Speedway, Stop C1400, Austin, Texas 78712, USA

⁹INAF Osservatorio Astronomico di Roma, Via Frascati 33,00040 Monteporzio (RM), Italy

¹⁰School of Physics & Astronomy, University of Nottingham, Nottingham NG7 2RD

¹¹Centre for Astronomy and Astrophysics, University of Lisbon, P-1349-018 Lisbon, Portugal

¹²Department of Astronomy, University of Massachusetts, Amherst, MA 01003, USA

¹³Max-Planck-Institut für extraterrestrische Physik, Giessenbachstrasse D-85748 Garching, Germany

¹⁴Department of Physics and Astronomy, Colby College, Waterville, ME, USA

¹⁵Institute of Cosmology and Gravitation, University of Portsmouth, Dennis Sciama Building, Burnaby Road, Portsmouth PO1 3FX, UK

¹⁶NOAO, 950 N. Cherry Avenue, Tucson, AZ 85719, USA

Accurate galaxy redshifts are vital to studying how the physical properties and environments of galaxies evolve over cosmic time. While high resolution, ground-based spectroscopy has traditionally provided the most reliable redshifts, these observations are time consuming for faint sources and are subject to the limited wavelength sensitivity of optical spectrographs, making it difficult to extent large redshift surveys beyond $z \sim 1.2$ (Davis et al. 2007; Lilly et al. 2007). Near-infrared (NIR) spectrographs are now pushing the redshift frontier into the so-called redshift desert (Trump et al. 2013; Sanders et al. 2014; Silverman et al. 2014; Wisnioski et al. 2014), however at these wavelengths ground based observations are subject to contamination from atmospheric OH lines. Photometric redshift estimates, on the other hand, can provide redshifts for large samples of galaxies, including relatively faint systems, at a lower observational cost compared to spectroscopy. However, even the best photometric redshifts have errors of a few percent and are subject to catastrophic outliers for rare sources, such as active galactic nuclei (AGN), if their unique spectral energy distributions (SED) and/or strong emission lines are not properly modeled a priori (Salvato et al. 2009, 2011).

Slitless grism spectroscopy with the Wide Field Camera 3 (WFC3) onboard the Hubble Space Telescope (*HST*) now provides a powerful alternative to ground-based spectroscopy and SED modeling for measuring distant redshifts. The slitless nature of the WFC3/IR grism offers the ability to obtain a spectrum of each galaxy in the detector's field-of-view, while the significantly reduced background levels compared to the ground means

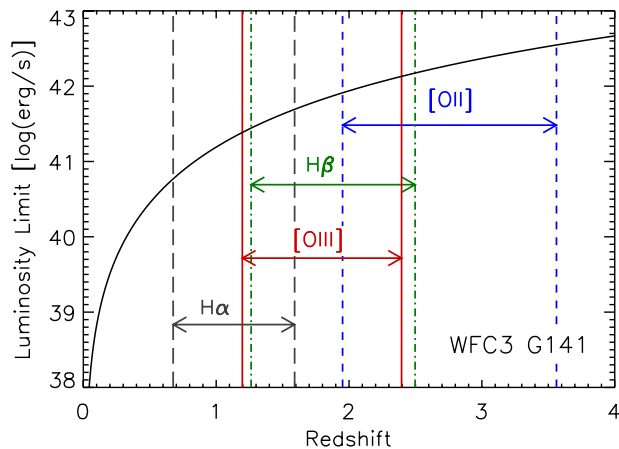


FIG. 1.— Line luminosity limits for detecting the $H\alpha$, $H\beta$, [OIII], and [OII] emission lines with 2 orbits of the *HST*/WFC3 G141 grism (corresponding to a line flux limit of 3×10^{-17} erg/s/cm²). Dashed vertical lines indicate the redshift ranges at which various lines are visible in the G141 sensitivity window (1.1-1.7 μ m).

emission lines can be detected for relatively faint galaxies with modest exposure times (e.g. Trump et al. 2011; Brammer et al. 2012; Straughn et al. 2011; Atek et al. 2011; van der Wel et al. 2011). In addition, the near-infrared sensitivity of WFC3 provides access to many important rest-frame optical emission lines over a wide range of redshifts, from $H\alpha$ down to $z = 0.7$ to [OII] $\lambda 3727$ at $z = 3.4$. Figure 1 shows the detectability of emission lines with 2-orbit depth G141 grism observations at various redshift ranges. Despite the low spectral resolution ($R \sim 130$) of the WFC3 grism, the resulting redshift accuracy is an order of magnitude better than typical photometric redshift errors (Brammer et al. 2012).

In this paper, we combine imaging and photometric redshifts from the Cosmic Assembly Near-Infrared Deep Extragalactic Legacy Survey (CANDELS; Grogin et al. 2011; Koekemoer et al. 2011) and WFC3/IR grism observations from the 3D-HST survey (Brammer et al. 2012) to produce a new grism spectroscopic redshift catalog for H -band selected galaxies in the GOODS-South field. The catalog contains emission-line redshifts for 608 sources which have no previously published spectroscopic redshifts and contains 234 new redshifts at $z > 1.5$. The paper is organized as follows: in Section 2 we introduce the datasets used in constructing the redshift catalog. In Section 3 we present the methodology used to inspect the grism spectra and measure redshifts. In Section 4 we present an overview of the redshift catalog and its key properties, provide an analysis of the accuracy of the redshift measurements, and use the new redshifts to identify close galaxy pair candidates. Finally, in Section 5 we summarize our work. Throughout this paper, we adopt the Chabrier IMF and the following cosmology: $H_0 = 70$ km s⁻¹ Mpc⁻¹, $\Omega_M = 0.3$, $\Omega_\Lambda = 0.7$. All magnitudes are in the AB system.

2. OBSERVATIONS AND SAMPLE SELECTION

2.1. Optical and Infrared Imaging

Our parent sample is drawn from the H -band selected photometric catalog of Guo et al. (2013), which made use of *HST*/WFC3 imaging of the GOODS-S field from three programs: CANDELS, the WFC3 Early Release

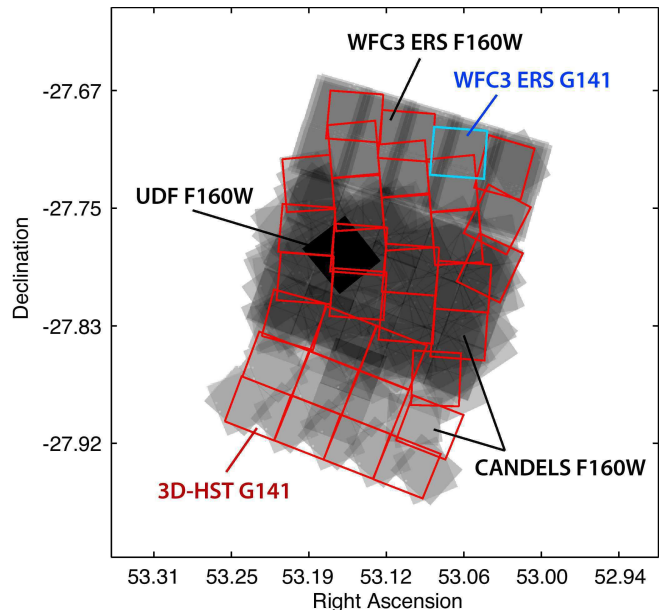


FIG. 2.— Layout in the GOODS-S field of the WFC3 F160W imaging and G141 grism observations used in this study. The imaging comes from the CANDELS, WFC3 ERS and HUDF09 programs, while the grism observations come from the 3D-HST (red) and WFC3 ERS programs (blue).

Science program (ERS; Windhorst et al. 2011), and the HUDF09 program (Bouwens et al. 2010). The location of the WFC3 imaging from these three programs is shown in Figure 2. CANDELS has observed GOODS-S using a two-tiered Wide+Deep strategy. The Deep region covers the central third of the GOODS-S area (55 arcmin²; Giavalisco et al. 2004) with 3, 4, and 6 orbits of F105W, F125W, and F160W imaging, respectively. The Wide region covers the southern third of the field with 2-orbit depth imaging in all three bands. The ERS program covers the northern third of GOODS-S with 2-orbit depth imaging in the F098M, F125W, and F160W bands. Finally, an area of 4.6 arcmin² in GOODS-S, the Hubble Ultra Deep Field, is covered by very deep 24, 34, and 53 orbits of F105W, F125W, and F160W imaging. The CANDELS team carried out a consistent reduction of the WFC3 imaging from all of these programs; for details we refer readers to Koekemoer et al. (2011).

The GOODS-S field has also been observed in the optical with the Advanced Camera for Survey (ACS) on *HST* as part of the GOODS *Hubble* Treasury Program (P.I. M. Giavalisco) in the B , v , i , and z bands with a total exposure time of 7200, 5450, 7028, and 18,232 seconds. For this study, we made use of the publicly available, version v3.0 mosaicked images from the GOODS Treasury Program. In the mid-infrared, we make use of *Spitzer*/IRAC 3.6 and 4.5 μ m imaging from the *Spitzer* Extended Deep Survey (SEDS; P.I. G. Fazio; Ashby et al. 2013), which reaches total 3σ depths of ~ 26 AB mag.

In addition to the observations described above, the GOODS-S region has been targeted for some of the deepest ground-based observations ever taken, ranging from the U band (Nonino et al. 2009) to the K band (Fontana et al. 2014). A detailed description of these datasets can be found in Grogin et al. (2011) and Guo et al. (2013).

2.2. Photometry and Photometric Redshifts

For this study, we make use of the CANDELS photometric catalog of Guo et al. (2013). The catalog is *H*-band selected using a “max-depth” image that combines all available F160W in the GOODS-S field. The catalog contains 34930 unique sources and is 50% complete at $H \sim 26$. Multiwavelength photometry is obtained for the available *HST* bands using a modified version of SExtractor (Bertin & Arnouts 1996; see Galametz et al. 2013) using the F160W observations as the detection image. For *Spitzer*/IRAC imaging and ground-based observations of mixed resolution, the TFIT software (Laidler et al. 2007) was employed to obtain PSF-matched photometry. Further details on the CANDELS multiwavelength photometry catalogs can be found in Guo et al. (2013) and Galametz et al. (2013).

Photometric redshifts for each source were generated from SED modeling using the photometry catalog of Guo et al. (2013). A hierarchical Bayesian approach was employed in which the full photometric redshift probability distribution from 11 independent CANDELS investigators are combined to produce a more accurate redshift estimate. The detailed description of this process can be found in Dahlen et al. (2013). The photometry used ranged from the *U*-band to the *Spitzer*/IRAC 4.5 μm filter; see Guo et al. (2013). The resulting photometric redshifts are found to be accurate to the 2.9% level and have an outlier fraction (OLF) of 9.1% when compared with a sample of available spectroscopic redshifts.

2.3. WFC3/IR Grism Data

GOODS-S contains near complete spectroscopic coverage in the NIR with 2-orbit depth *HST*/WFC3 G141 grism observations taken by the 3D-HST survey (PI: P. van Dokkum; Brammer et al. 2012) and the WFC3 ERS program (Straughn et al. 2011), corresponding to a limiting line flux of $3 \times 10^{-17} \text{erg/s/cm}^2$. The locations of the G141 observations in the GOODS-S field are shown in Figure 2. The publicly available data were reduced using the aXe software package (Kümmel et al. 2009) to produce two- and one-dimensional wavelength- and flux-calibrated spectra. Spectra were reduced using the default (V2.0) aXe parameters. This means we use a single sky background and do not account for the background fluctuations which typically affect the WFC3 grisms (Brammer et al. 2014). (The GOODS-S G141 observations have lower overall background than the other CANDELS / 3D-HST fields, although the GOODS-S background can vary from 1–2 e^-/s within a single pointing, see Appendix B of Brammer et al. 2012.) The extraction window was set to be four times the object size projected perpendicular to the dispersion direction, where object size is measured from the F140W image using SExtractor. The spectra each cover a wavelength range of $1.1 \leq \lambda \leq 1.7 \mu\text{m}$ with a resolving power $R \sim 130$ ($46.5 \text{\AA}/\text{pixel}$) for point sources. For each observation with the grism, an accompanying direct F140W image is taken to determine the wavelength zero-point for each spectrum. The uncertainty in the zero-point and the dispersion are 8\AA and $0.06 \text{\AA}/\text{pixel}$ respectively. The dispersion correlates to $\sim 1000 \text{ km s}^{-1}$ for $\text{H}\alpha$ at $z > 1$. The total exposure time for each F140W direct image is 812 s and the total exposure time for each G141 grism image

ranges between 4511 - 5111 s.

Finally, we registered the grism observations to the CANDELS imaging in the field by running SExtractor on the F140W direct images and cross-matched the resulting source catalog to the CANDELS F160W catalog of Guo et al. (2013). Through this cross-matching we derived an astrometric correction for each individual 3D-HST tile; the average derived correction was $0''.163$ in $\Delta\alpha$ and $0''.248$ in $\Delta\delta$.

2.4. Sample Selection

Our initial sample consists of 4511 sources selected from the catalog of Guo et al. (2013) based on the following criteria:

- *H*-band Magnitude: $H_{\text{F160W}} \leq 24$
- Photometric Redshift: $z_{\text{phot}} \geq 0.6$

These criteria are chosen such that prominent emission features fall within the sensitivity window of the G141 grism, but also such that the number of sources to be inspected does not become unmanageably large (e.g. increasing the magnitude cut to $H_{\text{F160W}} \leq 25$ more than doubles the sample size.) It is worth noting that as a result of these selection criteria, sources that are continuum-faint but have high-equivalent width emission lines may be missed from our initial selection. The same is true for sources with catastrophic failures in their photometric redshift estimates.

To determine which sources in our initial sample have preexisting spectroscopic redshifts, we compared the sample against a recent compilation of published spectroscopic redshifts in the GOODS-S field (N. Hathi, private communication). This compilation contains redshifts from various sources including Balestra et al. (2010); Cooper et al. (2012); Croom et al. (2001); Daddi et al. (2004); Huang et al. (2009); Kriek et al. (2007); Kurk et al. (2012); Le Fèvre et al. (2004); Mignoli et al. (2005); Ravikumar et al. (2007); Silverman et al. (2010); Strolger et al. (2004); Szokoly et al. (2004); Trump et al. (2013); van der Wel et al. (2004); Vanzella et al. (2008, 2009); Wolf et al. (2004); Wuyts et al. (2009); Xue et al. (2011), and the ESO GOODS/CDF-S Master Catalog¹. We refer to this compilation as the Master Spectroscopic Catalog hereafter. Based on this comparison, we define two samples: a primary sample consisting of 3007 sources which do not appear in the master spectroscopic catalog and a secondary sample of 1504 sources which have published spectroscopic redshifts. In the following sections, we analyze the grism spectra of both samples in an identical manner (i.e., with no prior knowledge of any published spectroscopic redshift) and use the secondary sample to test the accuracy of our grism-derived redshifts (see §4.2).

Of the 4511 sources in the initial sample, 2314 sources in the primary sample and 1226 sources in the secondary sample fall within the 3D-HST G141 footprint and are detected in the F140W imaging. For the sources in the primary sample, we extracted 2723 unique grism spectra from the 36 individual 3D-HST and ERS pointings, with 343 sources being identified in multiple pointings. We

¹ Available online at <http://www.eso.org/sci/activities/garching/projects/goods/MasterSpectroscopy.html>

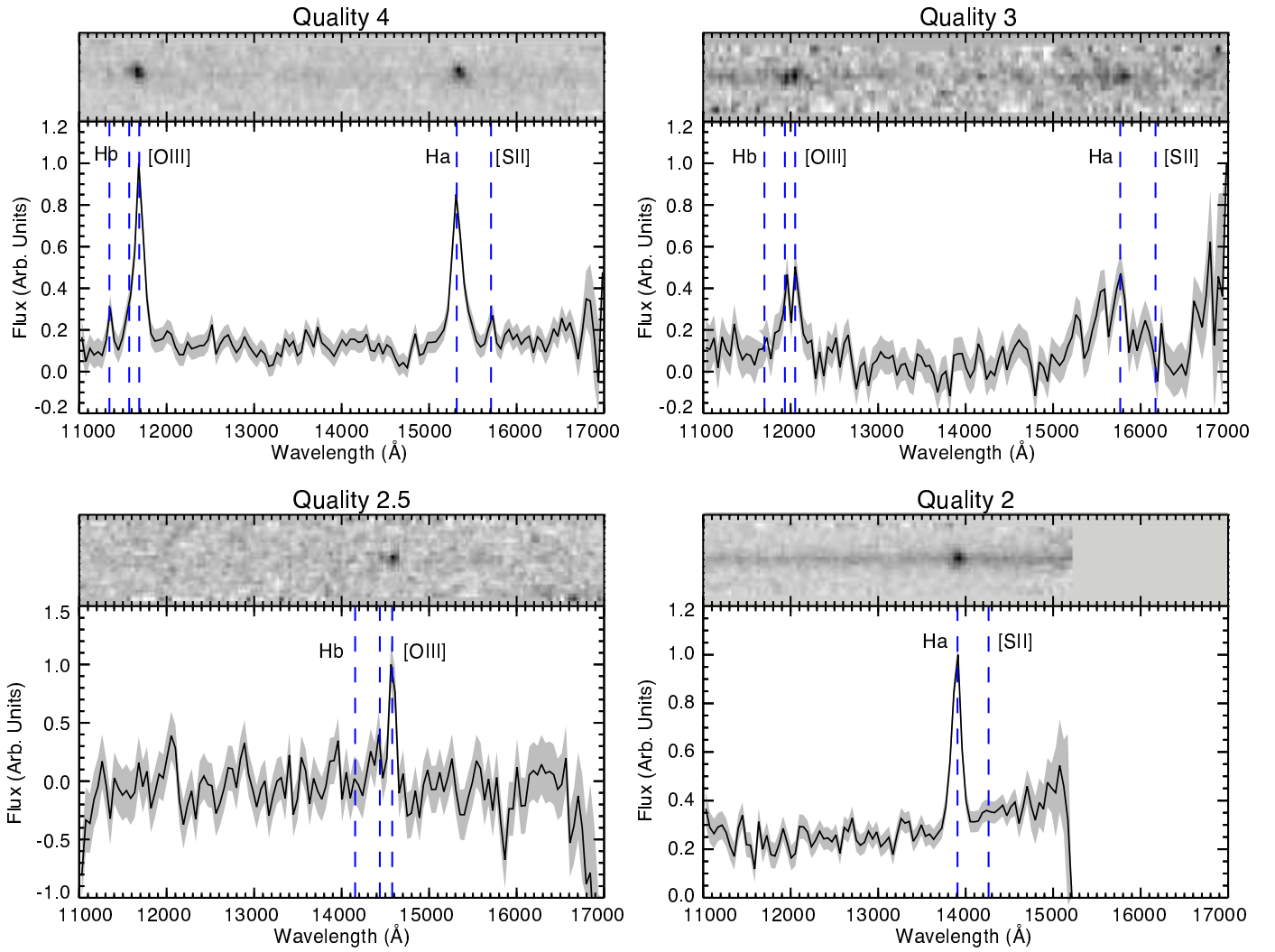


FIG. 3.— Examples of G141 grism spectra with quality flags 4.0 (multiple high S/N emission lines), 3.0 (multiple, lower S/N emission lines), 2.5 (single emission feature; redshift agrees with photometric redshift), and 2.0 (single emission feature; redshift disagrees with photometric redshift). Vertical dashed lines indicate the location of major emission features.

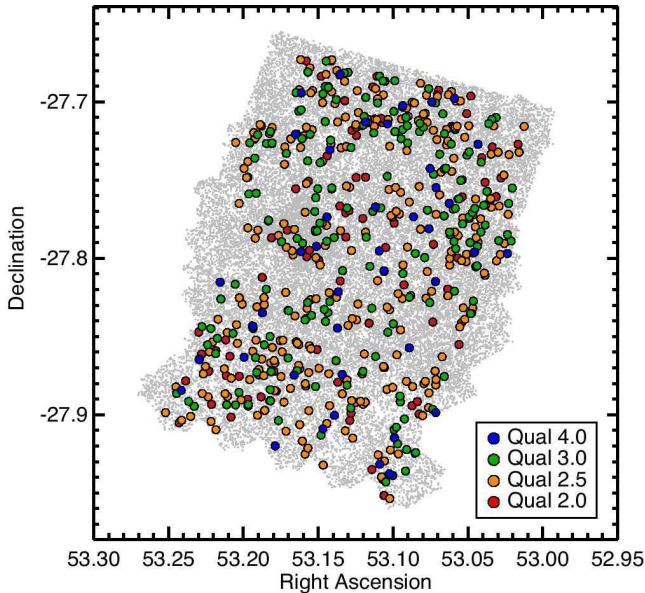


FIG. 4.— Distribution of sources with new grism redshifts in GOODS-S. Grey points are all sources from the catalog of Guo et al. (2013) and filled circles are sources with grism redshifts, color coded according to their assigned quality; see §3 for details.

extracted 1464 unique spectra for the secondary sample, with 224 sources being identified in multiple pointings.

3. REDSHIFT MEASUREMENT

The extracted 2D and 1D spectra for each object in our samples were visually inspected using the `SpecPro` IDL software package Masters & Capak 2011. In addition to the spectrum of each source, `SpecPro` also provides the user with the ability to display thumbnail images of the source being inspected, a plot of available photometry with an accompanying SED fit, and the location and width of the extraction window. To aid in the identification of emission lines, `SpecPro` provides the predicted location of various emission and absorption features based on the input photometric redshift for the source. Source spectra were also inspected for contamination from overlapping spectra using an estimate supplied by `aXe` which is indicated atop the 1D spectrum. It should be noted that no attempt was made to model or subtract contamination from each spectrum, although emission lines from neighboring sources were identified using the photometric or spectroscopic redshift of the contaminating source and contamination from zeroth order spectra is indicated by the contamination estimate supplied by `aXe`. Any source which exhibited excessive contamination or had data quality issues (e.g. significantly incomplete spectrum due to the spectrum being dispersed off the edge of the detector or spectra which overlap with defective portions of the detector) were removed from the sample. These sources accounted for roughly 17% of all 4187 extracted spectra in the primary and secondary samples.

During inspection, any visible spectral features were roughly fit manually and subsequently fit via cross-correlation with spectral templates provided in the software to determine the redshift of the source. `SpecPro`'s cross-correlation method is adapted from the cross-correlation routines originally written for the SDSS spectral reduction package, which follows the technique of Tonry & Davis 1979. When the automated

cross-correlation failed, the redshift was determined manually by fitting the peaks of the template emission features to those observed in the grism spectrum. This was done for less than 5% of sources. The templates used for cross-correlation are taken from the VVDS (Le Fèvre et al. 2005) and PEGASE Fioc & Rocca-Volmerange 1997 templates. The emission lines most often used for identification were $H\alpha$ /[NII] $\lambda\lambda 6550+6584$ and [SII] $\lambda\lambda 6717+6731$, $H\beta$ and [OIII] $\lambda\lambda 4959+5007$, and [OII] $\lambda 3727$. The spectral resolution of the grism is such that the above sets and duplexes are not resolved, but it is enough to produce certain distinguishing profiles that aid in differentiating each from other strong lines (e.g. the asymmetric profile of [OIII] $\lambda\lambda 4959+5007$.)

Upon inspection, the derived redshift of each source was assigned a quality flag based on the strength and number of the identified emission lines and the agreement with existing photometric redshift estimates. If a source was identified in multiple pointings and therefore assigned multiple redshifts, the higher quality redshift was always chosen. In the case where multiple redshifts of the same quality exist, the redshift of the source was taken to be the average of the individual redshifts. The quality scheme for the derived redshifts is as follows:

- 4.0: Multiple high S/N emission lines
- 3.0: Combination of high and low S/N emission lines.
- 2.5: Single high S/N emission line and redshift agrees with 68% confidence interval of photometric redshift
- 2.0: Single high S/N emission line and redshift does not agree with 68% confidence interval of photometric redshift

Examples of spectra correlating to each quality flag can be seen in Figure 3. While quality 3.0 and 4.0 redshifts are the most reliable, given the multiple emission lines identified, we show in §4.2 that sources assigned a quality of 2.0 or 2.5 demonstrate excellent agreement with prior spectroscopic redshift measurements.

4. RESULTS

4.1. Catalog Properties

Upon inspection and classification of the 2411 grism spectra in the primary sample, we have identified 608 sources with visible emission lines for which redshifts could be measured. Of these, 45 exhibited multiple high S/N emission lines (quality 4.0), 181 exhibited multiple emission lines with some low S/N emission lines (quality 3.0), 293 exhibited a single high S/N emission line whose redshift agrees with the 68% confidence interval of the CANDELS photometric redshift estimate (quality 2.5), and 89 exhibited a single high S/N emission line which does not agree with the 68% confidence interval of the photometric redshift (quality 2.0). In the secondary sample, we have identified 411 sources with visible emission lines for which redshifts could be measured. Of these, 35 exhibited multiple high S/N emission lines (quality 4.0), 167 exhibited multiple emission lines with some low S/N emission lines (quality 3.0), 157 exhibited a single high S/N emission line whose redshift agrees with the 68% confidence interval of the CANDELS photometric redshift estimate (quality 2.5), and 52 exhibited a single high S/N emission line which does not agree with

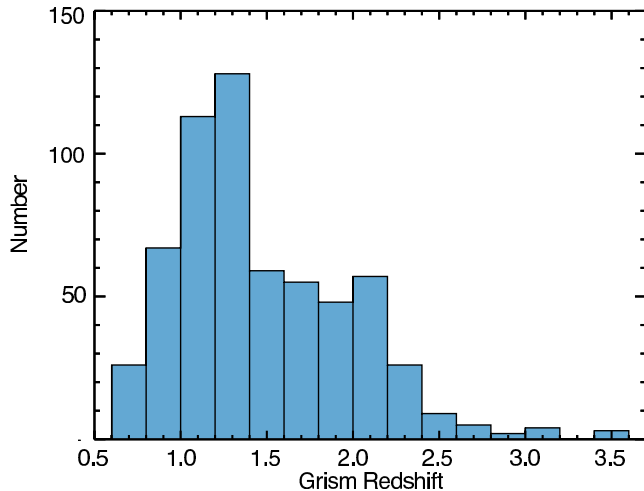


FIG. 5.— Distribution of the 608 new grism redshifts in GOODS-S. The redshifts span a range of $0.677 \leq z \leq 3.456$ and have a median redshift of $z = 1.282$. There are 234 sources with $z \geq 1.5$

the 68% confidence interval of the photometric redshift (quality 2.0).

The final catalog contains 1019 grism redshifts for galaxies brighter than $H = 24$ in the GOODS-S field. Roughly 60% (608/1019) of the redshifts are new, in that these galaxies have no previously published spectroscopic redshift. The new redshifts span a range of $0.677 \leq z \leq 3.456$ and have a median redshift of $z = 1.282$. The catalog contains a total of 234 new redshifts for galaxies at $z \geq 1.5$. The spatial distribution of the 608 galaxies with new redshifts can be seen in Figure 4 and their redshift distribution is shown in Figure 5. In addition, the stellar mass distribution of these 608 galaxies is shown in Figure 6. Here masses are calculated by SED modeling using photometry from the Guo et al. (2013) catalog as described in Mobasher et al. (2014, in prep.). We find that galaxies with new grism redshifts in our catalog are, on average, three times less massive than their counterparts with literature redshifts at $z \sim 1 - 2$.

Over the magnitude range of our primary sample ($H < 24$), we find that our ability to successfully measure a redshift is not strongly dependent on the H -band magnitude of the source. Figure 7 shows the magnitude distribution of sources in our primary sample along with the redshift success rate in each magnitude bin (defined as the ratio of the number of sources with grism redshifts of quality ≥ 2.0 to the number of all sources in our initial sample in a given bin). Over the magnitude range $22 < H < 24$, our success rate ranges from 20 to 30%, showing only a mild decrease for our faintest sources. Also shown in Figure 7 is our success rate as a function of redshift. Here we find a steady decrease from 35% to 10% in the redshift range $2.0 < z < 2.75$. This is likely due to [OIII] and $H\beta$ shifting beyond $1.7\mu\text{m}$ at $z = 2.4$ and 2.5, respectively, leaving [OII] as the single emission line visible in the G141 sensitivity window at $z > 2.5$.

We have investigated the nature of the sources for which a grism redshift could not be determined due to the lack of visible emission lines and find them to be a combination of bright, quiescent galaxies and faint star-forming systems. In Figure 8, we show the location of these galaxies on a UVJ diagram (Williams et al. 2009). This phase-space separates blue, star forming galaxies from redder

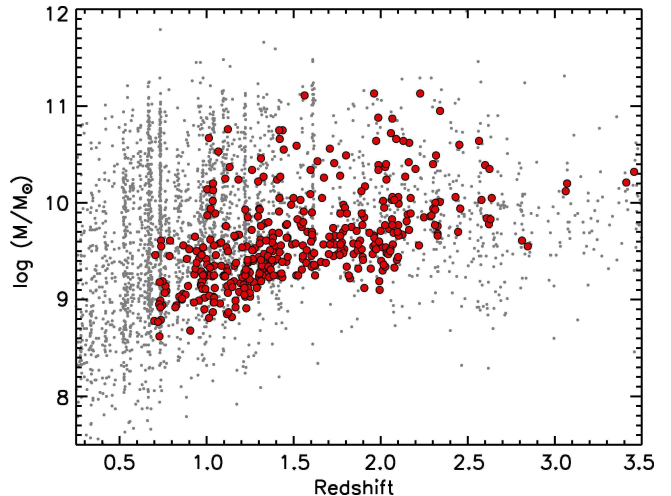


FIG. 6.— Mass distribution as a function of spectroscopic redshift for galaxies in the GOODS-S field. Galaxies with new grism redshifts from this work are shown as red circles, while galaxies with previously published spectroscopic redshifts are shown as grey points.

systems that are heavily dust extinguished or passively evolving. For this analysis, rest-frame colors were determined with the EAZY code (Brammer et al. 2008) using the observed photometry from Guo et al. (2013) and the CANDELS photometric redshift catalog. Of the galaxies which lack visible emission lines, we find that 33.0% are dusty or quiescent ($U - V_{\text{rest}} > 1.3$). This is nearly three times greater than the 12.4% of galaxies with measured grism redshifts that have similar rest-frame colors. The remaining 67.0% are blue, star-forming systems ($U - V_{\text{rest}} < 1.3$) that are predominately faint (64.5% are fainter than $H \sim 23$; the same is true for only 23.7% of the passive/dusty population). We therefore conclude that objects which failed to yield a grism redshift are largely a combination of quiescent galaxies that lack emission lines and star-forming galaxies with emission lines fainter than the detection limit of the grism observations.

4.2. Redshift Accuracy

To evaluate the accuracy of our measured redshifts, we first examine the agreement of the new grism redshifts with the CANDELS photometric redshifts. This is shown in the left panel of Figure 9. We quantify the accuracy of the catalog via the parameter σ_{NMAD} , defined as $1.48 \times \text{median}(|\Delta z|/(1 + z_{\text{phot}}))$. The grism redshifts show good agreement with the photometric redshifts, with $\sigma_{NMAD} = 0.0236$ and an OLF ($|\Delta z|/(1 + z_{\text{phot}}) \geq 0.15$) of 0.0150. These values are comparable to the accuracy of the photometric redshifts when compared against ground-based spectroscopic redshifts, so we may reasonably assume that the majority of this scatter is due to the error in the photometric redshifts. We believe many of the outliers in this evaluation are sources with SEDs contaminated by strong emission lines. A comparison to the work of Hsu et al. (2014), which takes into account intermediate-band *Subaru* photometry (Cardamone et al. 2010) and the contribution of emission lines in addition to the photometry presented in Guo et al. (2013), reduces the number of outliers in the sample from 9 to just 2.

To further assess the accuracy of the grism redshifts,

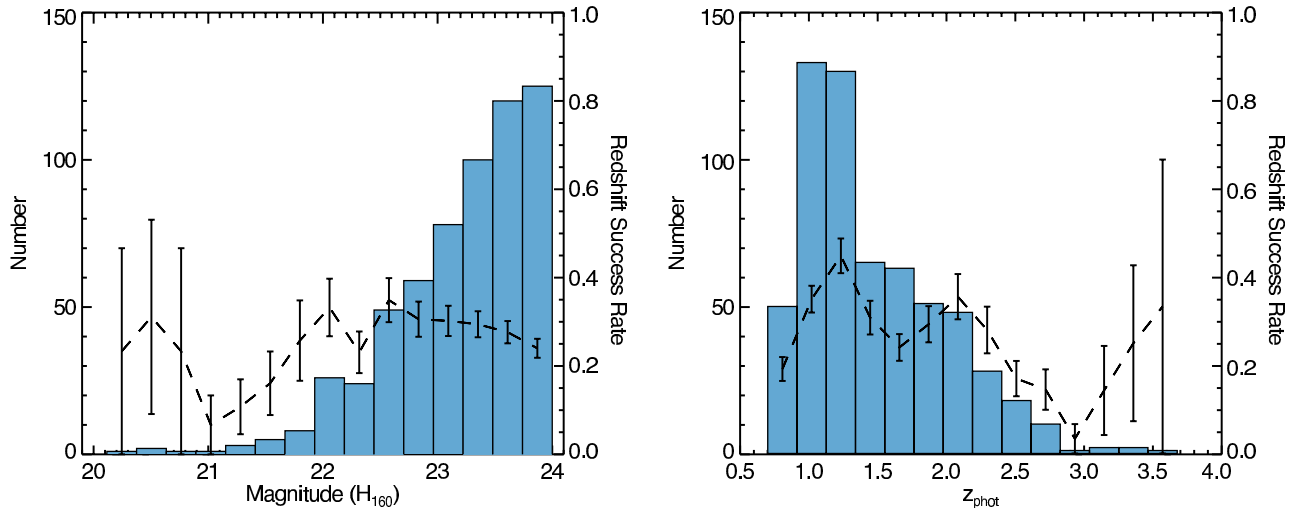


FIG. 7.— (left) Magnitude distribution of sources with new grism redshifts. The dashed line represents the redshift “success” rate in each bin with error bars given by number statistics based on the number of sources in that bin. (right) Redshift distribution of sources with new grism redshifts.

we examine the agreement of the secondary sample with the redshifts contained within the master spectroscopic catalog. Each extracted spectrum was inspected using the same methods employed for the primary sample; i.e., we used the photometric redshifts to aid in our redshift determination but had no knowledge of the published spectroscopic redshifts. This process resulted in 411 successful grism redshift determinations. A comparison of the grism and ground-based spectroscopic redshifts is shown on the right panel of Figure 9. This comparison yields a scatter of $\sigma_{NMAD} = 0.0028$ with an OLF of 0.0098. Compared to the work of Brammer et al. (2012), we find excellent agreement with the accuracy reported by the 3D-HST team ($\sigma_{NMAD} = 0.0035$).

As a further test of the accuracy of our catalog, we have compared our grism redshifts to those obtained by the WFC3 ERS program. Straughn et al. obtained 48 redshifts via their G102 and G141 observations, of which ten sources with the highest quality redshifts meet our magnitude and redshift selection criteria and received quality flags of 2.0 or higher in our inspection. We see excellent agreement between our results and those of Straughn et al., with a comparison in the manner described above giving a result of $\sigma_{NMAD} = 0.0016$.

We find that the scatter between the grism and ground-based spectroscopic redshifts is not significantly increased ($\Delta\sigma_{NMAD} \approx 0.0001$) for those sources whose redshifts were fit manually versus those fit via the built-in cross-correlation routines in *SpecPro*. We also find that the scatter does not vary significantly with quality flag, ranging from $\sigma_{NMAD} = 0.0026$ for quality 4 redshifts to $\sigma_{NMAD} = 0.0033$ for quality 2 redshifts. We therefore propose quality 2.0 as the minimum reliable quality for this redshift catalog. In addition, we find no correlation between scatter and the effective radius of the sources as defined in van der Wel et al. (2014).

4.3. Redshift Catalog

Starting with a sample of 4511 sources, we have obtained a total of 1019 grism redshifts for galaxies brighter than $H = 24$ in the GOODS-S field. Of these, 608 are new redshift measurements for galaxies in our primary

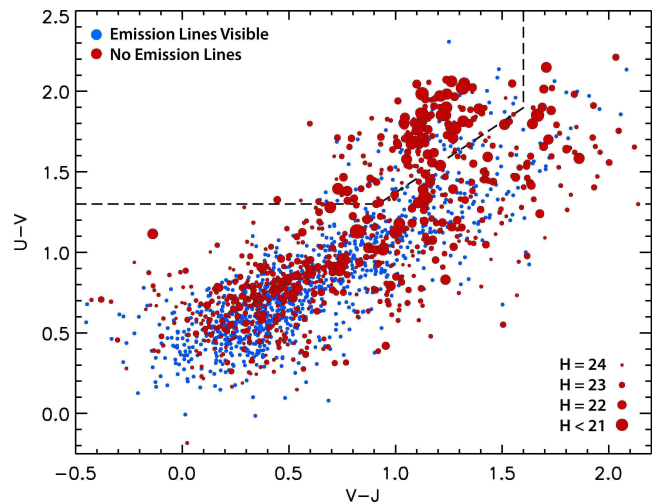


FIG. 8.— UVJ plot of rest-frame colors for all sources in both the primary and secondary samples. Blue points represent sources for which a grism redshift was successfully obtained and red sources represent sources for which a grism redshift was not obtained with point size scaled according to the source’s H -band magnitude. The dashed line separates the star-forming “blue cloud” and the quiescent “red sequence”. We find that sources without grism redshifts tend to be bright quiescent systems or faint star forming galaxies.

sample, which do not have previously published spectroscopic redshifts. The coordinates and redshifts of all 1019 galaxies are listed in Table 1. The details of the table columns are given below.

1. Source ID from Guo et al. (2013)
2. Right ascension (J2000)
3. Declination (J2000)
4. H -band magnitude (AB) from Guo et al. (2013)
5. Redshift derived from G141 grism spectrum
6. Redshift from Master Spectroscopic Catalog
7. Emission line(s) used for redshift determination
8. Redshift quality flag (see §3 for details)

4.4. Newly Identified Galaxy Pair Candidates

In this section, we highlight one of the potential uses for our redshift catalog, namely the identification of

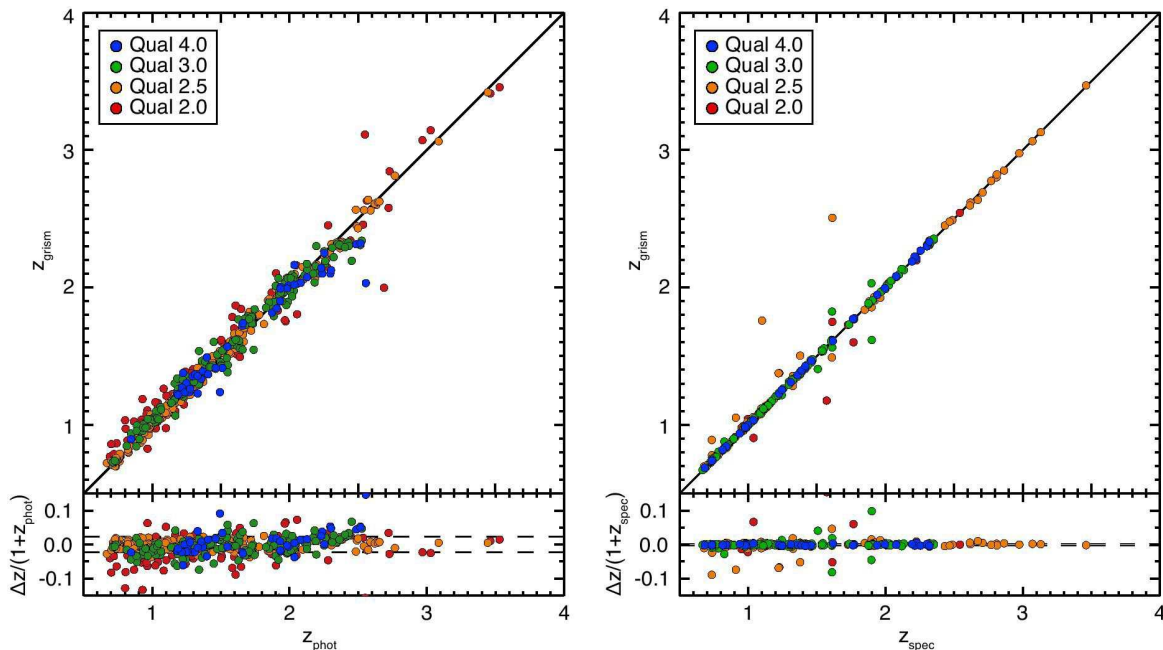


FIG. 9.— (*left*) Grism redshifts from this work versus CANDELS photometric redshifts. The solid line represents $z_{grism} = z_{phot}$, while the dashed lines represent $\sigma_{NMAD} = 0.0236$. (*right*) Grism redshifts from this work versus ground-based spectroscopic redshifts, with $\sigma_{NMAD} = 0.0028$.

close galaxy pairs at $z > 1$. Due to the slitless nature of the WFC3 grism, we can now dramatically increase the spectroscopic sampling of star forming galaxies at these redshifts. Even with a spectral resolution of $\delta v \sim 1000 \text{ km s}^{-1}$, the redshift accuracy of the G141 grism spectra ($\sigma_z / (1+z) = 0.3\%$) is far better than typical photometric redshift errors (3%) and the accuracy of low-resolution prism spectroscopy (1.2%), which have been used in the past to study the merger rate and environments of galaxies at $z \sim 1$ and beyond i.e., Patel et al. 2011; Newman et al. 2012.

Combining the grism redshifts in our catalog with our master spectroscopic catalog, we have identified 20 galaxy pair candidates in GOODS-S with at least one member whose redshift comes from the new WFC3/G141 spectra. To identify galaxy pairs, we inspect the neighbors of each galaxy with a grism redshift of quality 2.0 or greater and define close companions as those that are 1) within a projected distance of 50 kpc, and 2) have a redshift difference of $\Delta z / (1+z) < 0.03$, or roughly $\delta v \sim 1000 \text{ km s}^{-1}$ at $z > 1$. Based on these criteria, we find 20 galaxies with potential companions in the CANDELS/GOODS-S region. Five of the pairs are comprised of two galaxies with new grism redshifts and 15 are grism sources with companions that appear in our master spectroscopic catalog. The sample spans a redshift range of $0.787 \leq z \leq 2.33$, with four of the pairs identified at $z \sim 2$. This sample represents roughly a factor of two increase in the number of such pairs identified with the master spectroscopic catalog alone. On average, the new companions to sources with spectroscopic redshifts are nearly one magnitude fainter in the H -band, which highlights the ability of the grism to detect fainter objects than are usually seen via ground-based spectroscopy. In addition, the objects found in

these pairs are approximately ten times less massive than objects typically observed in pair studies at this redshift (López-Sanjuan et al. 2013; Tasca et al. 2014). The coordinates and redshifts of the newly detected pair candidates are listed in Table 2.

5. SUMMARY

We have constructed a redshift catalog for galaxies in the CANDELS/GOODS-S field using HST /WFC3 G141 grism observations from the 3D-HST survey and WFC3 ERS program. The G141 spectra cover a wavelength range of $1.1 \leq \lambda \leq 1.7 \mu\text{m}$, which allows for the detection of prominent emission lines over a wide redshift range, from $H\alpha$ at $z = 0.7$ to $[\text{OII}] \lambda 3727$ at $z = 3.4$. Our catalog is H -band selected based on the CANDELS photometry catalog of Guo et al. (2013). Spectra were extracted for all GOODS-S sources which are brighter than $H = 24$ and have a photometric redshift $z_{phot} \geq 0.6$. Each spectrum was visually inspected, emission lines were identified with the aid of CANDELS photometric redshifts, and redshifts were measured via cross-correlation with empirical spectral templates. Derived redshifts were assigned a quality ranging from 4.0 for sources with multiple strong emission lines, to 2.0 for sources with a single visible emission line. The resulting catalog contains new grism redshifts for 608 galaxies which have no previously published spectroscopic redshift in the GOODS-S field. These redshifts span a range of $0.677 \leq z \leq 3.456$ and include 234 new redshifts for galaxies at $z \geq 1.5$. The catalog also contains grism redshifts for 411 galaxies which have existing redshifts in the literature.

We find good agreement between our grism-derived redshifts and existing photometric redshifts from CANDELS ($\sigma_{NMAD} = 0.0236$). We've also tested the accuracy of our redshifts by extracting and inspecting the spectra of GOODS-S sources with published spectro-

scopic redshifts. This analysis was done blind, with only the photometric redshift of each source known during the inspection. Here we find excellent agreement between our redshifts and the published values ($\sigma_{NMAD} = 0.0028$). This agreement holds even for redshifts measured with only a single emission line (quality 2.5 and 2.0 in the catalog).

Finally, we use our redshift catalog to identify 20 new galaxy pair candidates at $z = 1 - 2$. These were chosen to have a projected separation of 50 kpc and a velocity offset of $\delta v \sim 1000 \text{ km s}^{-1}$. Included in this sample are four new pairs identified at $z \sim 2$.

This work is based on observations taken by the CANDELS Multi-Cycle Treasury Program (GO 12177) and the 3D-HST Treasury Program (GO 12328) with the NASA/ESA HST, which is operated by the Association of Universities for Research in Astronomy, Inc., under NASA contract NAS5-26555 and by the Spitzer Space Telescope, which is operated by the Jet Propulsion Laboratory, California Institute of Technology under a contract with NASA. We also acknowledge partial support from NSF 0808133 and HST-AR 12822.03-A.

TABLE 1 — *Continued*

Source ID (1)	RA (2)	Dec (3)	AB(F160W) (4)	z_{grism} (5)	z_{spec} (6)	Lines (7)	Qual (8)
1845	03 32 31.92	-27 54 03.1	23.76	2.489	2.487	[OII]	2.5
1846	03 32 49.98	-27 54 05.3	22.65	0.971	-	H α	2.0
1847	03 32 56.46	-27 54 03.8	23.21	1.663	-	[OIII]	2.5
1848	03 32 34.42	-27 54 05.6	21.25	1.076	1.088	H α	2.5
1855	03 32 19.29	-27 54 03.3	22.67	0.969	0.964	H α	2.5
1862	03 32 21.89	-27 54 03.1	22.16	1.010	1.001	H α	2.5
1875	03 32 33.40	-27 54 01.5	23.56	1.334	-	H β , [OIII], H α , [SII]	4.0
1907	03 32 45.74	-27 54 01.2	22.18	1.405	-	[OIII], H α , [SII]	2.5
1938	03 32 19.26	-27 54 01.9	20.83	1.122	-	H α	2.5
1942	03 32 19.82	-27 53 58.3	23.21	1.832	-	[OIII]	2.0
1977	03 32 30.73	-27 53 56.5	23.53	1.784	-	H β , [OIII]	2.0
1981	03 33 00.48	-27 53 55.1	23.65	1.596	-	[OIII]	2.5
1993	03 32 17.16	-27 53 54.8	23.64	1.353	-	[OIII], H α , [SII]	4.0
2029	03 32 22.52	-27 53 53.7	22.65	0.969	0.967	H α	2.5
2042	03 32 17.35	-27 53 52.8	22.68	1.361	1.359	H β , [OIII], H α , [SII]	4.0
2096	03 32 44.57	-27 53 50.2	23.69	1.090	-	H α	2.5
2100	03 32 37.51	-27 53 50.6	23.30	1.009	-	H α , [SII]	2.5
2192	03 32 17.65	-27 53 47.6	21.36	1.259	-	[OIII], H α	3.0
2206	03 32 18.30	-27 53 43.9	23.91	1.219	-	H α	2.5
2231	03 32 30.79	-27 53 44.5	22.98	1.784	-	H β , [OIII]	3.0
2265	03 32 40.80	-27 53 43.5	21.46	0.977	0.977	H α , [SII]	4.0
2278	03 32 55.87	-27 53 40.7	22.87	1.962	-	H β , [OIII]	3.0
2285	03 32 47.23	-27 53 39.8	23.37	2.161	-	[OIII]	2.0
2296	03 32 38.14	-27 53 39.9	23.14	2.814	2.811	[OII]	2.5
2311	03 32 34.18	-27 53 39.0	23.88	2.108	-	H β , [OIII]	2.5
2320	03 32 20.95	-27 53 39.2	22.52	1.437	-	[OIII]	2.0
2349	03 32 47.20	-27 53 36.5	23.49	1.791	-	H β , [OIII]	3.0
2359	03 32 49.26	-27 53 37.3	22.66	1.183	-	H α , [SII]	3.0
2361	03 32 50.68	-27 53 37.1	22.47	1.786	-	H β , [OIII]	3.0
2362	03 32 28.80	-27 53 35.9	23.55	0.984	-	H α	2.5
2364	03 32 53.12	-27 53 36.1	23.88	2.579	-	[OII]	2.0
2413	03 32 33.36	-27 53 33.4	23.24	0.683	0.679	H α , [SIII] λ 9532	3.0
2444	03 32 30.07	-27 53 32.0	22.74	1.220	-	H α	2.5
2454	03 32 28.45	-27 53 31.0	23.65	0.989	-	H α	2.5
2480	03 32 41.49	-27 53 31.0	23.95	1.276	-	[OIII], H α	2.5
2486	03 32 20.11	-27 53 29.7	23.37	1.187	-	H α	2.0
2508	03 32 46.21	-27 53 29.0	22.89	1.386	1.385	H α	2.0
2513	03 32 22.85	-27 53 30.3	23.26	1.882	-	H β , [OIII]	3.0
2520	03 32 30.64	-27 53 27.6	23.83	1.729	-	[OIII]	2.5
2524	03 32 43.77	-27 53 27.5	23.61	1.458	-	[OIII], H α	3.0
2526	03 32 43.66	-27 53 28.0	23.46	1.465	-	[OIII], H α	3.0
2551	03 32 56.79	-27 53 29.3	22.09	1.423	-	H α , [SII]	3.0
2583	03 32 29.21	-27 53 29.0	22.42	1.033	-	H α	2.5
2590	03 32 48.37	-27 53 25.9	23.02	0.797	-	H α	2.5
2614	03 32 47.31	-27 53 24.1	22.57	1.295	-	H α	2.0
2674	03 32 34.60	-27 53 24.4	21.36	1.105	1.107	H α , [SII]	3.0
2697	03 32 57.98	-27 53 22.4	21.87	1.032	1.035	H α , [SII]	3.0
2724	03 32 53.64	-27 53 18.9	23.29	0.745	-	H α	2.5
2744	03 32 50.55	-27 53 18.1	22.54	1.614	-	[OIII]	2.5
2755	03 32 22.87	-27 53 17.1	23.69	1.752	-	H β , [OIII]	3.0
2766	03 32 45.17	-27 53 19.1	22.47	1.783	-	[OIII]	2.0
2844	03 32 42.56	-27 53 13.5	23.32	1.312	1.296	[OIII], H α	3.0
2864	03 32 32.14	-27 53 11.9	23.28	0.981	-	H α	2.5
2887	03 32 54.60	-27 53 11.0	23.76	1.612	-	[OIII]	2.5
2889	03 32 50.94	-27 53 11.9	23.09	0.942	-	H α	2.5
2903	03 32 58.43	-27 53 10.8	22.90	1.026	1.034	H α	2.5
2909	03 32 33.34	-27 53 12.8	21.75	0.697	0.679	H α	2.5
2923	03 32 58.70	-27 53 11.0	23.46	1.896	-	H β , [OIII]	3.0
2954	03 32 48.70	-27 53 08.6	23.20	1.975	-	H β , [OIII]	3.0
2976	03 32 18.26	-27 53 09.8	21.93	1.127	-	H α	2.5
3022	03 32 42.74	-27 53 05.6	23.57	0.858	-	H α	2.5
3052	03 32 57.95	-27 53 03.9	23.77	1.366	-	H β , [OIII], H α	4.0
3081	03 32 43.01	-27 53 04.5	23.30	0.879	-	H α	2.5
3107	03 32 43.68	-27 53 02.3	23.48	1.308	-	H α , [SII]	3.0
3146	03 32 24.98	-27 53 01.8	23.28	1.120	-	H α	2.5
3200	03 32 40.45	-27 52 59.2	23.00	1.795	-	[OIII]	2.5
3251	03 32 58.82	-27 52 56.0	24.00	1.905	-	[OIII]	2.5
3279	03 32 24.06	-27 52 57.2	21.94	1.132	-	H α	2.5
3281	03 32 36.43	-27 52 55.1	23.92	1.624	-	H β , [OIII]	3.0
3315	03 32 38.01	-27 52 53.9	23.53	1.006	-	H α	2.5
3344	03 32 20.86	-27 52 55.2	22.35	0.830	-	H α	2.5
3347	03 32 21.08	-27 52 52.6	23.22	2.801	2.807	[OII]	2.5
3380	03 32 41.84	-27 52 53.8	23.28	1.095	1.102	H α	2.5
3389	03 32 31.41	-27 52 51.8	23.78	1.770	-	H β , [OIII]	3.0
3432	03 32 19.05	-27 52 48.3	23.98	1.039	-	H α , [SII]	2.5

TABLE 1 — *Continued*

Source ID (1)	RA (2)	Dec (3)	AB(F160W) (4)	z_{grism} (5)	z_{spec} (6)	Lines (7)	Qual (8)
16844	03 32 10.89	-27 46 05.3	22.97	2.302	–	H β , [OIII]	3.0
16848	03 32 14.00	-27 46 05.1	23.52	0.727	–	H α , [SII] λ 9532	3.0
16865	03 32 28.07	-27 46 06.0	22.35	1.113	1.109	H α	2.5
16881	03 32 26.17	-27 46 03.5	23.48	1.220	1.221	H α , [SII]	3.0
16897	03 32 12.60	-27 46 05.0	23.29	1.365	1.378	H α	2.5
16905	03 32 15.74	-27 46 04.3	22.19	1.532	1.537	H α	2.5
16936	03 32 25.99	-27 46 04.1	22.97	1.003	–	H α , [SII]	3.0
16937	03 32 08.24	-27 46 02.5	23.34	1.084	–	H α	2.5
16958	03 32 31.38	-27 46 04.3	23.07	2.089	–	H β , [OIII]	3.0
16970	03 32 26.82	-27 46 01.8	23.67	2.074	–	[OII], H β , [OIII]	4.0
16985	03 32 22.54	-27 46 03.7	22.77	1.727	1.727	[OIII]	2.0
17006	03 32 24.15	-27 46 00.2	22.86	0.893	0.893	H α , [SII]	3.0
17027	03 32 36.91	-27 46 02.3	23.56	2.308	2.321	[OII], H β , [OIII]	3.0
17069	03 32 32.54	-27 45 59.8	22.78	0.969	–	H α	2.0
17071	03 32 06.98	-27 45 59.9	22.37	1.327	–	H α	2.5
17073	03 32 09.45	-27 45 58.4	23.47	2.318	–	H β , [OIII]	3.0
17151	03 32 09.14	-27 45 56.9	23.17	2.331	–	[OIII]	2.5
17165	03 32 36.32	-27 46 00.0	22.30	0.899	0.895	H α , [SII]	3.0
17172	03 32 35.46	-27 45 56.2	23.72	2.318	2.325	[OII], H β , [OIII]	3.0
17213	03 32 21.23	-27 45 54.8	23.40	1.223	1.224	[OIII], H α , [SII]	3.0
17214	03 32 37.29	-27 45 57.8	22.43	1.099	1.096	H α	2.5
17221	03 32 21.31	-27 45 54.6	23.61	1.222	1.223	[OIII], H α	3.0
17233	03 32 25.66	-27 45 55.5	22.78	1.032	1.040	H α , [SII]	3.0
17235	03 32 05.45	-27 45 54.0	23.09	1.160	–	H α , [SII]	3.0
17244	03 32 22.70	-27 45 54.6	22.90	0.846	–	H α , [SII]	3.0
17251	03 32 48.67	-27 45 53.9	22.95	1.305	–	H α	2.5
17259	03 32 06.40	-27 45 54.7	21.74	1.332	1.329	H α	2.5
17265	03 32 04.72	-27 45 54.9	21.92	1.076	1.076	H α	2.5
17290	03 32 14.99	-27 45 53.4	22.92	1.235	–	[OIII], H α , [SII]	4.0
17297	03 32 14.95	-27 45 54.4	22.80	1.230	–	H α , [SII]	3.0
17316	03 32 43.48	-27 45 56.4	21.32	1.219	1.220	H α	2.0
17376	03 32 12.20	-27 45 54.3	21.34	1.033	1.038	H α	2.5
17386	03 32 23.15	-27 45 54.6	21.31	1.226	1.223	H α	2.5
17415	03 32 21.39	-27 45 50.5	23.64	1.916	–	H β , [OIII]	2.5
17422	03 32 16.84	-27 45 51.0	22.80	1.032	1.018	H α	2.5
17472	03 32 27.39	-27 45 49.5	22.48	0.724	0.727	H α	2.5
17482	03 32 06.84	-27 45 50.2	21.27	0.848	0.846	H α	2.5
17488	03 32 20.17	-27 45 49.3	23.20	1.614	1.611	H β , [OIII]	3.0
17500	03 32 08.42	-27 45 46.8	23.50	1.609	–	[OIII]	2.5
17509	03 32 35.79	-27 45 49.0	22.70	0.749	0.738	H α	2.5
17528	03 32 22.24	-27 45 50.3	21.84	0.730	0.726	H α , [SII]	3.0
17593	03 32 17.75	-27 45 47.6	21.60	0.736	0.735	H α	2.0
17594	03 32 13.58	-27 45 43.7	23.99	0.721	–	H α	2.5
17605	03 32 22.63	-27 45 46.7	22.15	0.830	0.840	H α	2.5
17608	03 32 13.44	-27 45 43.4	23.56	0.843	–	H α , [SII]	3.0
17612	03 32 10.77	-27 45 43.8	23.93	0.729	–	H α	2.5
17617	03 32 08.36	-27 45 42.8	23.76	1.222	–	H α , [SII]	2.5
17652	03 32 10.94	-27 45 44.5	22.25	1.033	1.039	H α , [SII]	4.0
17655	03 32 28.59	-27 45 42.0	23.58	1.824	1.611	H β , [OIII]	3.0
17698	03 32 36.40	-27 45 40.6	23.29	0.996	–	H α , [SII]	3.0
17705	03 32 26.73	-27 45 39.9	23.42	2.010	2.006	H β , [OIII]	3.0
17757	03 32 07.48	-27 45 38.4	23.76	2.631	–	[OII]	2.0
17824	03 32 41.34	-27 45 38.2	21.80	1.540	1.539	H β , [OIII], H α	3.0
17843	03 32 12.93	-27 45 38.6	22.30	1.053	–	H α	2.0
17849	03 32 13.93	-27 45 37.2	22.10	0.844	0.841	H α , [SII]	3.0
17932	03 32 16.54	-27 45 34.2	23.35	0.893	–	H α	2.5
17937	03 32 24.66	-27 45 33.6	23.07	2.318	2.312	[OII], H β , [OIII]	4.0
17943	03 32 47.13	-27 45 31.9	23.59	1.304	–	[OIII], H α , [SII]	3.0
17973	03 32 45.95	-27 45 30.6	23.92	1.435	–	[OIII], H α , [SII]	3.0
17994	03 32 26.77	-27 45 30.5	23.79	1.122	1.122	H α	2.0
18023	03 32 21.72	-27 45 29.7	23.46	2.076	2.080	H β , [OIII]	3.0
18068	03 32 22.78	-27 45 28.1	23.43	1.987	–	[OIII]	2.5
18085	03 32 03.37	-27 45 25.4	25.27	2.318	0.316	H β , [OIII]	3.0
18095	03 32 08.97	-27 45 26.3	23.57	2.025	–	[OII], H β , [OIII]	3.0
18109	03 32 08.90	-27 45 26.0	23.95	2.017	–	[OIII]	2.5
18132	03 32 17.49	-27 45 28.2	21.72	1.042	1.039	H α , [SII]	3.0
18160	03 32 39.26	-27 45 32.2	20.67	1.118	1.095	H α	2.5
18177	03 32 12.48	-27 45 30.4	21.91	1.372	1.375	H α , [SII]	3.0
18213	03 32 33.15	-27 45 22.7	23.92	1.930	1.918	[OIII]	2.5
18240	03 32 28.90	-27 45 25.2	22.50	0.978	0.952	H α	2.0
18243	03 32 05.49	-27 45 25.2	21.52	1.191	1.189	H α	2.5
18315	03 32 33.84	-27 45 20.5	23.50	2.310	–	[OII], [OIII]	3.0
18334	03 32 36.07	-27 45 19.7	23.49	2.302	–	[OII], [OIII]	3.0
18343	03 32 05.95	-27 45 20.4	22.40	0.978	0.974	H α	2.5
18369	03 32 37.88	-27 45 18.7	23.27	0.910	0.906	H α	2.0

TABLE 1 — *Continued*

Source ID (1)	RA (2)	Dec (3)	AB(F160W) (4)	z_{grism} (5)	z_{spec} (6)	Lines (7)	Qual (8)
20180	03 32 35.70	-27 44 19.9	23.19	0.936	—	H α , [SII]	3.0
20189	03 32 09.85	-27 44 19.1	23.82	2.172	—	H β , [OIII]	3.0
20213	03 32 26.13	-27 44 18.8	23.22	2.030	2.021	—	2.0
20219	03 32 22.58	-27 44 25.8	19.48	0.743	0.738	H α	2.5
20237	03 32 20.11	-27 44 22.4	21.09	1.210	1.217	H α , [SII]	3.0
20239	03 32 42.05	-27 44 21.2	21.90	1.150	1.152	H α	2.5
20242	03 32 47.28	-27 44 17.4	23.90	2.149	—	[OII], [OIII]	2.5
20299	03 32 35.34	-27 44 19.2	22.42	1.232	1.224	H α	2.5
20341	03 32 35.32	-27 44 17.2	23.58	1.331	—	H α	2.5
20343	03 32 10.18	-27 44 16.3	22.66	2.309	2.304	[OIII]	2.5
20357	03 32 37.69	-27 44 16.1	22.15	1.214	—	H α , [SII]	3.0
20403	03 32 33.77	-27 44 17.4	22.18	1.309	1.299	H α	2.5
20447	03 32 10.91	-27 44 14.9	21.54	2.506	1.613	[OII]	2.5
20482	03 32 46.18	-27 44 09.5	23.69	1.963	—	H β , [OIII]	3.0
20495	03 32 11.86	-27 44 13.3	21.40	1.282	1.325	H α	2.5
20522	03 32 09.77	-27 44 08.8	23.45	0.859	—	H α	2.0
20534	03 32 45.74	-27 44 09.7	23.49	1.144	1.142	H α	2.5
20540	03 32 24.01	-27 44 08.2	23.48	1.614	1.610	H β , [OIII]	3.0
20579	03 32 14.28	-27 44 09.7	23.26	0.970	—	H α	2.5
20587	03 32 14.98	-27 44 08.1	23.51	2.637	2.673	[OII]	2.5
20628	03 32 24.64	-27 44 07.6	21.97	1.617	1.901	H β , [OIII]	3.0
20636	03 32 46.91	-27 44 06.8	21.69	1.141	1.146	H α , [SII]	3.0
20639	03 32 37.40	-27 44 06.9	21.43	1.024	1.017	H α	2.5
20694	03 32 34.57	-27 44 04.5	22.70	0.933	—	H α	2.0
20742	03 32 12.15	-27 44 02.6	23.67	1.250	—	H α , [SII]	3.0
20780	03 32 05.41	-27 44 01.6	22.48	0.790	—	H α	2.5
20795	03 32 16.52	-27 44 00.4	23.25	1.260	—	H α , [SII]	3.0
20831	03 32 08.27	-27 44 00.4	23.24	1.600	—	[OIII]	2.5
20834	03 32 45.18	-27 44 01.3	23.31	1.925	1.962	[OIII]	2.5
20861	03 32 41.11	-27 43 58.5	23.27	2.191	—	[OII], H β , [OIII]	3.0
20920	03 32 46.34	-27 43 56.5	22.96	0.984	0.979	H α , [SII]	4.0
20927	03 32 03.79	-27 43 56.1	23.07	0.956	—	H α	2.5
21004	03 32 11.82	-27 43 55.2	23.17	1.231	—	[OIII], H α	3.0
21056	03 32 21.80	-27 43 52.3	23.92	1.309	—	H α	2.5
21098	03 32 31.52	-27 43 50.8	23.41	2.189	2.193	[OII], H β , [OIII]	4.0
21112	03 32 34.13	-27 43 50.3	23.75	1.992	—	[OII], H β , [OIII]	4.0
21118	03 32 05.12	-27 43 51.0	22.18	0.809	0.807	H α , [SII]	2.0
21123	03 32 32.14	-27 43 49.8	22.58	0.980	0.973	H α	2.0
21133	03 32 07.16	-27 43 55.9	20.97	1.217	—	H α	2.5
21162	03 32 23.95	-27 43 49.0	22.22	1.310	1.311	[OIII], H α , [SII]	4.0
21226	03 32 32.33	-27 43 45.8	23.37	1.022	—	H α	2.5
21236	03 32 43.63	-27 43 47.7	22.80	2.316	2.313	[OII], [OIII]	3.0
21258	03 32 30.74	-27 43 45.3	23.30	1.434	—	H β , [OIII], H α , [SII]	3.0
21282	03 32 10.69	-27 43 46.9	22.43	1.356	1.327	H α	2.5
21299	03 32 41.34	-27 43 44.1	23.02	0.984	—	H α , [SII]	2.5
21307	03 32 31.50	-27 43 42.7	23.87	2.097	—	[OIII]	2.5
21321	03 32 38.83	-27 43 44.9	22.47	1.227	—	H α	2.5
21329	03 32 24.53	-27 43 42.3	23.02	1.088	—	H α	2.5
21354	03 32 08.10	-27 43 44.1	21.74	1.211	—	H α	2.0
21398	03 32 03.49	-27 43 40.5	23.88	3.129	3.132	[OII]	2.5
21464	03 32 47.02	-27 43 46.4	21.00	1.179	1.178	H α	2.5
21527	03 32 10.39	-27 43 37.6	23.21	1.991	—	[OII], H β , [OIII]	4.0
21564	03 32 43.46	-27 43 36.5	23.45	2.078	—	H β , [OIII]	3.0
21568	03 32 17.51	-27 43 36.5	23.41	1.610	1.608	[OIII]	2.5
21579	03 32 33.96	-27 43 36.7	23.27	1.352	—	H α	2.5
21594	03 32 14.68	-27 43 37.0	22.42	0.979	—	H α , [SII]	3.0
21612	03 32 44.30	-27 43 35.7	23.69	1.430	—	H β , [OIII]	3.0
21616	03 32 15.41	-27 43 39.4	22.03	1.563	—	[OIII]	2.5
21624	03 32 21.65	-27 43 34.5	23.89	2.036	—	H β , [OIII]	3.0
21679	03 32 43.41	-27 43 34.6	23.52	2.172	—	H β , [OIII]	3.0
21681	03 32 49.24	-27 43 33.6	22.78	1.169	—	H α	2.5
21688	03 32 03.98	-27 43 37.4	20.60	0.969	—	H α	2.0
21699	03 32 46.98	-27 43 34.4	22.35	1.259	—	[OIII], H α , [SII]	3.0
21786	03 32 04.37	-27 43 31.1	22.49	2.267	2.256	[OII], H β , [OIII]	4.0
21792	03 32 17.27	-27 43 29.7	23.25	1.896	1.905	[OIII]	2.5
21826	03 32 15.21	-27 43 30.0	22.88	0.747	—	H α	2.5
21839	03 32 34.01	-27 43 28.2	23.63	1.602	—	H β , [OIII]	3.0
21885	03 32 16.97	-27 43 26.8	23.11	0.734	—	H α	2.5
21888	03 32 10.95	-27 43 29.7	21.38	1.216	1.215	H α , [SII]	3.0
21923	03 32 46.24	-27 43 26.3	23.61	1.247	—	H α	2.5
21932	03 32 40.40	-27 43 25.4	23.99	1.248	—	[OIII]	2.5
21933	03 32 41.96	-27 43 27.0	23.17	0.778	0.767	H α , [SII]	2.5
21963	03 32 38.60	-27 43 24.6	23.28	1.043	—	H α , [SII]	3.0
21985	03 32 13.34	-27 43 24.3	23.34	1.296	1.297	[OIII], H α	3.0
22005	03 32 40.33	-27 43 24.6	22.32	1.254	1.245	[OIII], H α , [SII]	4.0

TABLE 1 — *Continued*

Source ID (1)	RA (2)	Dec (3)	AB(F160W) (4)	z_{grism} (5)	z_{spec} (6)	Lines (7)	Qual (8)
25793	03 32 28.38	-27 41 49.9	22.76	1.767	—	H β , [OIII]	3.0
25833	03 32 11.54	-27 41 46.7	22.65	1.489	—	[OIII]	2.0
25839	03 32 18.91	-27 41 37.4	23.98	2.300	2.306	[OII], H β	3.0
25841	03 32 16.88	-27 41 47.4	23.98	1.526	—	[OIII]	2.5
25850	03 32 18.64	-27 41 44.4	23.00	1.330	—	H α	2.5
25870	03 32 27.25	-27 41 25.7	23.33	2.457	—	[OII]	2.0
25878	03 32 18.94	-27 41 51.8	21.08	0.978	0.976	H α , [SII]	3.0
25888	03 32 27.43	-27 41 54.4	23.05	0.958	0.968	H α	2.5
25896	03 32 14.14	-27 41 52.1	23.12	2.320	—	[OII], H β , [OIII]	4.0
25915	03 32 26.47	-27 41 53.0	23.43	1.295	—	H α , [SII]	2.5
25966	03 32 33.32	-27 42 03.9	23.69	1.709	—	[OIII]	2.5
26050	03 32 13.89	-27 41 58.2	22.62	1.313	—	H α	2.5
26068	03 32 13.19	-27 41 58.0	22.37	1.302	—	H α	2.5
26085	03 32 17.77	-27 42 00.4	23.52	1.740	—	H β , [OIII]	4.0
26110	03 32 32.85	-27 41 55.7	23.32	0.953	0.951	H α	2.5
26134	03 32 20.92	-27 42 00.8	23.76	1.705	—	[OIII]	2.5
26135	03 32 31.75	-27 41 57.4	22.00	1.962	—	[OIII]	2.0
26136	03 32 34.90	-27 41 52.8	23.45	2.306	2.313	[OII], H β , [OIII]	3.0
26185	03 32 35.29	-27 42 01.8	22.35	1.086	—	H α	2.5
26209	03 32 33.12	-27 41 54.9	22.39	0.956	—	H α , [SII]	3.0
26213	03 32 18.27	-27 42 04.1	22.51	0.850	0.848	H α , [SII]	3.0
26222	03 32 26.80	-27 41 56.3	22.18	1.617	1.614	[OIII]	2.5
26255	03 32 34.60	-27 42 01.2	21.81	1.046	1.042	H α , [SII]	3.0
26294	03 32 22.42	-27 42 08.9	23.70	1.217	—	[OIII], H α , [SII]	4.0
26300	03 32 33.83	-27 41 36.8	22.30	1.051	—	H α	2.5
26301	03 32 26.33	-27 42 09.6	22.41	0.936	0.938	H α , [SII]	4.0
26306	03 32 20.58	-27 42 02.7	23.77	1.336	—	H α	2.5
26330	03 32 37.67	-27 42 06.6	22.68	0.850	—	H α	2.0
26364	03 32 26.48	-27 42 02.2	23.77	1.769	—	H β , [OIII]	3.0
26491	03 32 21.84	-27 42 13.8	23.56	1.019	—	H α	2.5
26518	03 32 22.51	-27 42 12.0	23.54	1.312	—	[OIII], H α	3.0
26552	03 32 17.67	-27 42 08.8	22.54	1.187	1.188	H α	2.5
26554	03 32 33.87	-27 42 03.9	21.38	1.607	1.604	H β , [OIII]	3.0
26629	03 32 39.26	-27 42 19.2	22.28	1.770	1.764	H β , [OIII]	4.0
26637	03 32 25.16	-27 42 18.7	21.43	1.610	1.617	H β , [OIII]	4.0
26699	03 32 38.75	-27 42 18.3	22.79	1.433	—	H β , H α	3.0
26704	03 32 29.56	-27 42 24.7	22.80	0.969	—	H α	2.5
26751	03 32 37.68	-27 42 19.3	22.19	1.437	1.436	H α , [SII]	3.0
26755	03 32 34.28	-27 42 24.9	20.20	1.090	1.088	H α	2.5
26788	03 32 23.88	-27 42 22.1	23.15	1.420	—	H α , [SII]	3.0
26801	03 32 21.60	-27 42 33.2	23.56	1.768	—	[OIII]	2.5
26823	03 32 16.03	-27 42 27.7	23.69	2.022	—	H β , [OIII]	3.0
26829	03 32 12.19	-27 42 27.0	22.55	0.734	—	H α	2.0
26833	03 32 13.75	-27 42 55.8	23.98	2.638	—	[OII]	2.5

NOTE. — [OII] and [OIII] in column 7 above refer always to the [OII] $\lambda\lambda 3727+3729$ and [OIII] $\lambda\lambda 4959+5007$ emission line doublets.

TABLE 2
GRISM-IDENTIFIED PAIRS IN GOODS-S

Source ID 1 (Guo+ 2013)	Source ID 2 (Guo+ 2013)	RA Source 1	Dec Source 1	RA Source 2	Dec Source 2	z_1	z_2	Angular Sep. (arcsec)	Proj. Sep. (kpc)	Mass Ratio M_1/M_2
722	726	53.096496	-27.925050	53.096385	-27.925972	1.145	1.146	3.338	27.48	0.847
1708	1695	53.241265	-27.903526	53.241173	-27.903265	1.050	1.045	0.984	7.963	1.086
2524	2526	53.182411	-27.890996	53.181927	-27.891138	1.458	1.465	1.623	13.72	0.974
3606	3689	53.078473	-27.878643	53.078256	-27.878455	0.987	0.987	0.967	7.720	0.981
3707	3952	53.071376	-27.877464	53.072763	-27.876321	1.099	1.100	6.034	49.31	0.845
5948	5983	53.055988	-27.855096	53.056169	-27.855367	1.227	1.226	1.133	9.426	0.948
6223	6195	53.173546	-27.852423	53.175354	-27.852610	0.967	0.962	5.794	45.99	0.971
7129	7172	53.193578	-27.843512	53.193960	-27.843195	2.003	2.011	1.668	13.96	1.011
8472	8452	53.114217	-27.831856	53.113214	-27.832735	1.295	1.293	4.495	37.64	0.951
10987	11071	53.093517	-27.809712	53.093552	-27.809287	2.327	2.334	1.534	12.56	0.963
11160	11218	53.105939	-27.808401	53.106022	-27.807946	2.014	2.020	1.659	13.87	1.007
16113	16275	53.100546	-27.773643	53.101308	-27.772737	1.014	1.016	4.066	32.68	0.952
18095	18109	53.037376	-27.757329	53.037104	-27.757242	2.025	2.017	0.921	7.701	1.044
18967	18795	53.156543	-27.750777	53.157256	-27.751523	1.605	1.607	3.517	29.80	0.908
21681	21576	53.205173	-27.726024	53.205371	-27.726181	1.169	1.163	0.847	6.994	1.091
21839	21897	53.141731	-27.724507	53.142011	-27.724565	1.602	1.602	0.916	7.761	0.956
21932	22005	53.168360	-27.723737	53.168083	-27.723513	1.248	1.245	1.196	9.971	0.949
22795	23970	53.058673	-27.716358	53.059861	-27.716288	1.023	1.022	3.794	30.54	0.979
23632	24274	53.117190	-27.713409	53.116405	-27.712703	1.618	1.610	3.566	30.21	0.868
24564	24904	53.135636	-27.682839	53.136296	-27.683073	0.787	0.787	2.266	16.92	0.974

REFERENCES

- Ashby, M. L. N., Willner, S. P., Fazio, G. G., et al. 2013, *ApJ*, 769, 80
- Atek, H., Siana, B., Scarlata, C., et al. 2011, *ApJ*, 743, 121
- Balestra, I., Mainieri, V., Popesso, P., et al. 2010, *A&A*, 512, A12
- Bertin, E., & Arnouts, S. 1996, *A&AS*, 117, 393
- Bouwens, R. J., Illingworth, G. D., Oesch, P. A., et al. 2010, *ApJ*, 709, L133
- Brammer, G., Pirzkal, N., McCullough, P., & MacKenty, J. 2014, Time-varying Excess Earth-glow Backgrounds in the WFC3/IR Channel, Tech. rep.
- Brammer, G. B., van Dokkum, P. G., & Coppi, P. 2008, *ApJ*, 686, 1503
- Brammer, G. B., van Dokkum, P. G., Franx, M., et al. 2012, *ApJS*, 200, 13
- Cardamone, C. N., van Dokkum, P. G., Urry, C. M., et al. 2010, *ApJS*, 189, 270
- Cooper, M. C., Yan, R., Dickinson, M., et al. 2012, *MNRAS*, 425, 2116
- Croom, S. M., Warren, S. J., & Glazebrook, K. 2001, *MNRAS*, 328, 150
- Daddi, E., Cimatti, A., Renzini, A., et al. 2004, *ApJ*, 600, L127
- Dahlen, T., Mobasher, B., Faber, S. M., et al. 2013, *ApJ*, 775, 93
- Davis, M., Guhathakurta, P., Konidaris, N. P., et al. 2007, *ApJ*, 660, L1
- Fioc, M., & Rocca-Volmerange, B. 1997, *A&A*, 326, 950
- Fontana, A., Dunlop, J. S., Paris, D., et al. 2014, *ArXiv e-prints*, arXiv:1409.7082
- Galametz, A., Grazian, A., Fontana, A., et al. 2013, *ApJS*, 206, 10
- Giavalisco, M., Ferguson, H. C., Koekemoer, A. M., et al. 2004, *ApJ*, 600, L93
- Grogin, N. A., Kocevski, D. D., Faber, S. M., et al. 2011, *ApJS*, 197, 35
- Guo, Y., Ferguson, H. C., Giavalisco, M., et al. 2013, *ApJS*, 207, 24
- Hsu, L.-T., Salvato, M., Nandra, K., et al. 2014, *ArXiv e-prints*, arXiv:1409.7119
- Huang, J.-S., Faber, S. M., Daddi, E., et al. 2009, *ApJ*, 700, 183
- Koekemoer, A. M., Faber, S. M., Ferguson, H. C., et al. 2011, *ApJS*, 197, 36
- Kriek, M., van Dokkum, P. G., Franx, M., et al. 2007, *ApJ*, 669, 776
- Kümmel, M., Walsh, J. R., Pirzkal, N., Kuntschner, H., & Pasquali, A. 2009, *PASP*, 121, 59
- Kurk, J., Cimatti, A., Daddi, E., et al. 2012, *VizieR Online Data Catalog*, 354, 99063
- Laidler, V. G., Papovich, C., Grogin, N. A., et al. 2007, *PASP*, 119, 1325
- Le Fèvre, O., Vettolani, G., Paltani, S., et al. 2004, *A&A*, 428, 1043
- Le Fèvre, O., Guzzo, L., Meneux, B., et al. 2005, *A&A*, 439, 877
- Lilly, S. J., Le Fèvre, O., Renzini, A., et al. 2007, *ApJS*, 172, 70
- López-Sanjuan, C., Le Fèvre, O., Tasca, L. A. M., et al. 2013, *A&A*, 553, A78
- Masters, D., & Capak, P. 2011, *PASP*, 123, 638
- Mignoli, M., Cimatti, A., Zamorani, G., et al. 2005, *A&A*, 437, 883
- Newman, A. B., Ellis, R. S., Bundy, K., & Treu, T. 2012, *ApJ*, 746, 162
- Nonino, M., Dickinson, M., Rosati, P., et al. 2009, *ApJS*, 183, 244
- Patel, S. G., Kelson, D. D., Holden, B. P., Franx, M., & Illingworth, G. D. 2011, *ApJ*, 735, 53
- Ravikumar, C. D., Puech, M., Flores, H., et al. 2007, *A&A*, 465, 1099
- Salvato, M., Hasinger, G., Ilbert, O., et al. 2009, *ApJ*, 690, 1250
- Salvato, M., Ilbert, O., Hasinger, G., et al. 2011, *ApJ*, 742, 61
- Sanders, R. L., Shapley, A. E., Kriek, M., et al. 2014, *ArXiv e-prints*, arXiv:1408.2521
- Silverman, J. D., Mainieri, V., Salvato, M., et al. 2010, *ApJS*, 191, 124
- Silverman, J. D., Kashino, D., Arimoto, N., et al. 2014, *ArXiv e-prints*, arXiv:1409.0447
- Straughn, A. N., Kuntschner, H., Kümmel, M., et al. 2011, *AJ*, 141, 14
- Strolger, L.-G., Riess, A. G., Dahlen, T., et al. 2004, *ApJ*, 613, 200
- Szokoly, G. P., Bergeron, J., Hasinger, G., et al. 2004, *ApJS*, 155, 271
- Tasca, L. A. M., Le Fèvre, O., López-Sanjuan, C., et al. 2014, *A&A*, 565, A10
- Tonry, J., & Davis, M. 1979, *AJ*, 84, 1511
- Trump, J. R., Weiner, B. J., Scarlata, C., et al. 2011, *ApJ*, 743, 144
- Trump, J. R., Konidaris, N. P., Barro, G., et al. 2013, *ApJ*, 763, L6
- van der Wel, A., Franx, M., van Dokkum, P. G., & Rix, H.-W. 2004, *ApJ*, 601, L5
- van der Wel, A., Straughn, A. N., Rix, H.-W., et al. 2011, *ApJ*, 742, 111
- van der Wel, A., Franx, M., van Dokkum, P. G., et al. 2014, *ApJ*, 788, 28
- Vanzella, E., Cristiani, S., Dickinson, M., et al. 2008, *A&A*, 478, 83
- Vanzella, E., Giavalisco, M., Dickinson, M., et al. 2009, *ApJ*, 695, 1163
- Williams, R. J., Quadri, R. F., Franx, M., van Dokkum, P., & Labbé, I. 2009, *ApJ*, 691, 1879
- Windhorst, R. A., Cohen, S. H., Hathi, N. P., et al. 2011, *ApJS*, 193, 27
- Wisnioski, E., Förster Schreiber, N. M., Wuyts, S., et al. 2014, *ArXiv e-prints*, arXiv:1409.6791
- Wolf, C., Meisenheimer, K., Kleinheinrich, M., et al. 2004, *A&A*, 421, 913
- Wuyts, S., van Dokkum, P. G., Franx, M., et al. 2009, *ApJ*, 706, 885
- Xue, Y. Q., Luo, B., Brandt, W. N., et al. 2011, *ApJS*, 195, 10